AIP Conference Proceedings

Preparation and simulation of lead mix-halide perovskite solar cells

Aqel Mashot Jafar, Falah Mustafa Al-Attar, Khalil I. Inad, Amar Moula Hmood, Saad Mahdi Saleh, and Kawther A. Khalaph

Preparation and Simulation of Lead Mix-halide Perovskite Solar Cells

Aqel Mashot Jafar[1,a)], Falah Mustafa Al-Attar[1)], Khalil I. Inad[1)], Amar Moula Hmood[2)], Saad Mahdi Saleh[1)] and Kawther A. Khalaph [3)]

[1]*Solar Energy Research Center, Renewable Energy Directorate, Higher Education and Scientific Research Ministry, Baghdad, Iraq.*
[2]*Materials Researches Directorate, Higher Education and Scientific Research Ministry, Baghdad, Iraq*
[3]*College of Science for women, Baghdad University, Higher Education and Scientific Research Ministry, Baghdad, Iraq.*

[a)]Corresponding author: aqel.jafar@yahoo.com

Abstract. The Organic Perovskite Solar Cells (OPSCs) exhibit several distinctive properties of their optoelectronic response. In this paper, OPSCs which have harvesting light of materials, $MAPbIBr_2$ and $MAPbICl_2$, with Cu_2O as hole transport materials (HTM) were synthesized. Optical and structural properties for the peroveskite materials and HTM layers of OPSCs were investigated. Finally, the I-V curves of the OPSCs were measured via Integrated cell tester included the I-V Photovoltaic measurements system and the Solar simulator system. The Power Conversion Efficiencies (PCE) of OPSCs were (3.22%) and (2.49%) to the devices which have $MAPbIBr_2$ or $MAPbICl_2$ as absorption layers, respectively. Measurements were tested at light Intensity ($100Wm^{-2}$)).

INTRODUCTION

In the past decade, perovskite materials have been attracted researchers with great interest because of their electrical, optical properties and good catalysts, which have important in solar cell applications. OPSCs were considered highly efficient and easy manufacture in simple ways from low cost materials [1]. Many researchers in previous literatures have studied in detail of experimental part and how to prepare solar cells. Copper oxide (Cu_2O), a semiconductor of known P-type material, was studied as HTM of OPSCs and contributed to reducing the energy loss due to higher mobility of Cu_2O, low Cu_2O/perovskite interface recombination loss, and better perovskite crystallinity on Cu_2O film. OPSCs –based on Cu_2O demonstrate a good performance of the photo-voltaic devices by improving the open-circuit voltage and the high short current of the test report of solar profile cells, thus improving the efficiency of the energy conversion to OPSCs. [2]. In the literatures survey, Several researchers detailed studied theoretical predictions in perovskite solar cells using computational programs such as VESTA and Gaussian programs. The lattice structures of the Perovskite materials were investigated and analyzed through the study of the density function theory (DFT) [3,4]. Therefore, the researchers deem that the correlation between the experimental data of optical properties and its compatibility with the theoretical study of the energy gaps and the bands of VBM and CBM of Perovskite materials have been not studied in the previous literature. Hence, in the current work, the fit studying between the empirical data of the optical and structural properties of the Perovskite materials and the theoretical data of obtained parameters of these properties using Gaussian 09 package have been conducted, and comparative studying have been achieved. The structural and optical properties of the perovskite, ETM and HTM layers were investigated with computational calculations characterized by detailed electronic properties through the Gaussian_09W_9.5_Revision_D.01 and Chem3D Ultra 10.0 programs. Harte-Fock with DFT was employed to calculate and characterize parameters as energy level of highest occupied molecular orbital (HOMO), energy level of lowest unoccupied molecular orbital (LUMO) and HOMO-LUMO energy gap. In addition, the simple methods

of deposition of HTM, ETM and Perovskite materials such as electrophoretic deposition technique (EPD), drop casting method for OPSCs were prepared in the present work.

BASIC THEORY

The optical properties of perovskite thin films were studied. The Absorption coefficient (α), were measured as function of energy of photon incident. Equation (2) is based on the Beer-Lambert law for optical absorption, where I_o is the intensity of the incident light and I is the intensity of the transmitted light of the film with thickness (t), Absorbance (A), and the Absorption coefficient (α) which shown in the following equation [5]:

$$\alpha = \frac{1}{t} * ln\left(\frac{I_o}{I}\right) = 2.303 * \frac{A}{t} \qquad (1)$$

We calculated the direct optical band gap ,E_g, of the perovskite thin films from the equation (2)   [6]:

$$hv * \alpha = B * \left[hv - E_g\right]^{1/2} \qquad (2)$$

Where, h is the Planck constant, (α) is the absorption coefficient , v is the light frequency , E_g is the optical energy gap and B is empirical constant. The open voltage circuit (V_{oc}) of Photovoltaic solar cells can be expressed as function of E_g as the following equation.

$$qV_{oc} = E_g - E_{loss} \qquad (3)$$

Where q represents the elementary charge and E_{loss} denotes to the loss in potential.

COMPUTATIONAL CALCULATIONS

In this research, the experimental results of FTIR were enhanced with the analysis of the Chem3D Ultra 10.0 program. The program of Gaussian 09W 9.5 Revision D.01 was employed to investigate the optimized of molecular structure in the unit cell of the crystal of the perovskite materials. An addition, the optical properties of this materials were confirmed with the electronic results of Gauss-View 5.0 program as HOMO and LUMO electrons distribution and the HOMO-LUMO energy gap. The Ground States, Hartree-Fock with SDD, method was chosen to get the best of data analysis of perovskite compounds. Both of the Perdew–Burke–Ernzerhof (PBE) exchange–correlation functional and the Heyd– Scuseria–Ernzerhof (HSE) hybrid functional were used to calculated the band structures and density of states of ABX_3[3]. The valence band is found to be made up by an anti-bonding linear combination of B s states and X p states, whereas the bands made up by the p anti-bonding states of B p and X p dominate the bottom of conduction band. The strong anti-bonding Bs–X p state may be more delocalized than the X p of the perovskite solar cell[3]. In the present work, we were computed the density of states(DOS) of Perovskite materials ABX_3 (A=CH_3NH_3; B= Pb; X=Cl, Br, I) and estimated band gap energy by using of the equation (4)[7].

$$DOS = \sum_{l=0}^{1} \sum_{i=1}^{\infty} \sqrt{\frac{(2l+1)!}{4\pi}} \left(\frac{1}{2^l l!}\right) |\langle\alpha_i|\beta_i\rangle|^2 E_i \qquad (4)$$

Where $\langle\alpha i | \beta i \rangle$ is overlap integral, αi and βi are the matrixes coefficients of Molecular Orbital of Alpha electron with spin (1/2) and Beta electron with spin (-1/2), respectively. E_i is eigenvalues of energy matrix and l is angular momentum ($l = 0,1$).

EXPERIMENTAL

Preparation of Organic Perovskite Materials (OPM) is reported in Ref [8,9, 10 and 11]. Methylamine Iodide (CH_3NH_3I) is prepared by reacting 24ml of Methylamine in 100 ml of   Ethanol (BDH-LTD) with 10 ml of Hydro-Iodic acid (HI) 57% of weight in water (BDH-LTD) under ice bath stirring for 1 h. following by drying at

100 °C, a white powder is formed, which is placed overnight in a vacuum oven before use. To obtain the perovskite precursor solution, we dissolved both 0.158 g of the CH_3NH_3I and 0.122g of the $PbBr_2$ (BDH-LTD) in anhydrous N,N DiMethyl Formamide (DMF) (Sigma Aldrich). 10 ml of solution preparation added to 0.15 g of Nano particle> 30 nm of Al_2O_3 powder (China of origin) to obtain precursor solution as scaffold peroveskite of $CH_3NH_3IPbBr_2$. As the same method, we dissolved both 0.158 g of the CH_3NH_3I and 0.092 g of the $PbCl_2$ (BDH-LTD) in (DMF). 10 ml of solution preparation added to 0.15 g of Nano particle> 30 nm of Al_2O_3 powder to obtain precursor solution as scaffold peroveskite of $CH_3NH_3IPbCl_2$. The reactions is described as the folowing equations:

$$CH_3NH_3I + PbBr_2 \xrightarrow{DMF} CH_3NH_3PbIBr_2 \qquad (5)$$

$$CH_3NH_3I + PbCl_2 \xrightarrow{DMF} CH_3NH_3PbICl_2 \qquad (6)$$

Preparation of compact layer ZnO of photo-electrode is a first fabricated by employment Aerosol Assisted Chemical Vapor Deposition (AACVD) technique via using Ultrasonic Atomizer (402AI) with ultrasonic frequency (1.5MHz) [5]. The precursor solution, which preparation of Nano particle> 20 nm of ZnO powder (China of origin) dispersed in ethanol solvent, is sprayed on per-heated Transparent Conductive Oxide (TCO) glass substrates of Fluorine-doped Tin Oxide (FTO) (Coated Sodaline float glass of Visiontek, sheet Resistance 8 Ω/□) at 450 ºC, deposited time is 1h. The hot substrates are left to cold at room temperature, followed by, depositing scaffold peroveskite precursor solution of CH3NH3PbX3 by spin coating at speed 2000 rpm and annealing at 100^0C to obtain 2 samples of (FTO/Compact ZnO /ScaffoldCH3NH3PbX3) as shown in figure (1-a) which depicts the structure thin films of PhotoVoltaic (PV) device and figure (1-b) depicts the image of PV device. The temperature of the (FTO/Compact ZnO) coated substrates is monitored by an infrared temperature digital indicator through the all experimental runs. Counter electrod is preparation by imployment Electrophoretic deposition (EPD) [12] to deposited thin film of Cu_2O on FTO electrode. To prepare the aqueous solution of Cu_2O, 3.18 g of Cu_2O is dissolving in 100 ml of 0.3M of Lactic Acid CH3CH(OH)COOH and equivalent ph = 4 via adding belts of NaOH. The electrolytic cell is a glass beaker containing the electrodes suspended in the Cu_2O aqueous solution. The counter electrode consists of a square foil of Cu and the working electrode is FTO with the same geometry. Both electrodes had a specific surface of 4 cm^2.
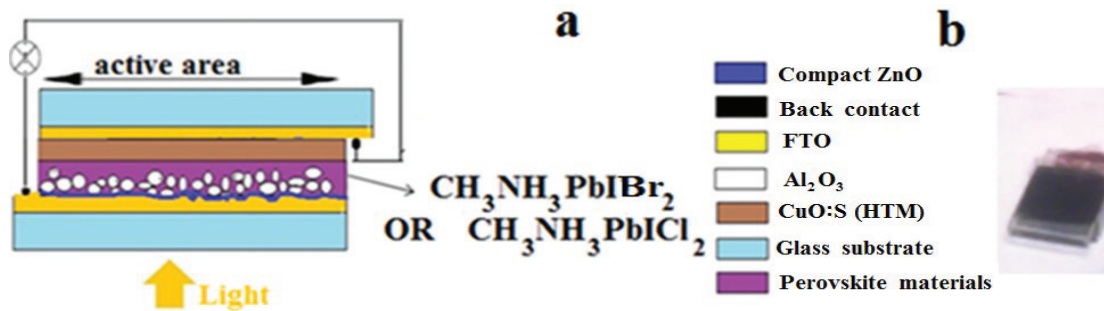

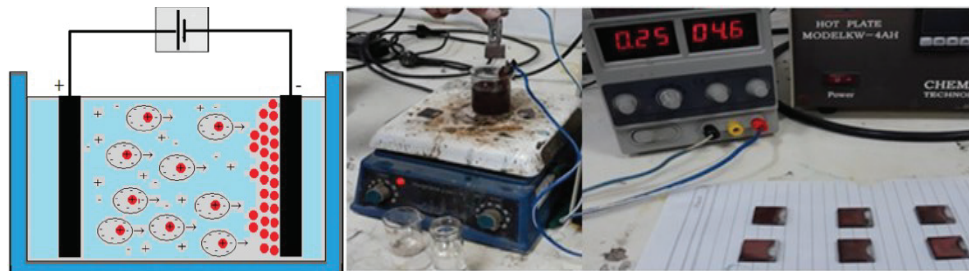**FIGURE 1. a:** The structure thin films of PV device, **b**: image of PV device.

FIGURE 2. The image of (EPD) method.

The electrodes are assembled to a Digital power supply and maintained at a constant distance of 2 cm. The Cu_2O aqueous solution was stirred with a magnetic stirrer at low speed to avoid aggregation during the deposition process. All of the experiments at constant current density conditions at 50 ºC temperatures. EPD experiments runs were carried out applying Voltage (4.6 Volts) and current densities (62 mA/cm^2) for 15 sec, as shone in figure (2).

Followed by, the sample is dipping in deionized water and dipping in 0.4M of CuS aqueous solution and anealing to 100 °C at 15 min. Scaffold peroveskite precursor solutions of CH3NH3IPbBr$_2$ or CH3NH3IPbCl$_2$ are drop casting process on the samples of (FTO/Compact TiO$_2$ /Scaffold CH$_3$NH$_3$PbX$_3$) and assemble individually with Cu$_2$O counter electrode followed by annealing at 100°C to obtain 2 samples of solar cells with configuration (FTO / Compact TiO2 / Scaffold CH$_3$NH$_3$IPbBr$_2$ or CH$_3$NH$_3$IPbCl$_2$ / Cu$_2$O / FTO) , as showed in figure (1).

CHARACTERIZATION OF CELLS, PERFORMANCE AND MEASUREMENTS EQUIPMENT'S

Composition and crystal structure studied by X- Ray Diffraction (XRD Shimadzu 6000, Cu-Kα) for perovskite coating. The structures of the perovskite crystals studied by images of Scanning Electron Microscope (SEM) (Bruker Nano GmbH, Germany). Light I-V Measurement Test Reports are recorded by Photovoltaic measurements system, composed of Oriel I−V test station using an Oriel Solar simulator. The solar simulator is class AAA for spectral performance, uniformity of irradiance, and temporal stability. The solar simulator is equipped with a 450 W xenon lamp. The output power is adjusted to match AM1.5 global sunlight (100 mW cm^{-2}). I−V curves are obtained by applying an external bias to the cell and measuring the generated photocurrent with a Keithley model 2400 digital source meter .The transmittance of coated films is measured in the wavelength range of (400 - 800) nm using a (SPECTRO UV/Vis Double Beam (UVD-3500) Labomed ,Inc). A blank sample of substrate is used as a reference in the measurement of optical transmittance. The transmittance of the powder samples is measured in the wavenumber at range of (0 - 4000) cm^{-1} by using a (SPECTRO FTIR TENSOR 27).

RESULTS AND DISCUSSION

Structural Studies

The FTIR spectral feature and peak positions for the Methyl Amine Ioded (MAI), as standard data, are computed via Chem3D Ultra 10.0 program and plotted in figure(3), data with black line ; C–N stretching vibrations from MAI at 1020-1220 cm^{-1}; N–H stretching in the range about 1560 cm^{-1} – 3500 cm^{-1}; C–H stretching both located at 2920 cm^{-1} [13]. The FTIR spectral of MAI prepared at the Present Work (P. W.), data curve with pink line, can be confirmed and identified of the spectral of FTIR data which calculated as the results of Chem3D Ultra 10.0 program, as showed in figure (3). The sample of the MAI pawder preparation is tested at the rang of the wave number (0-4000)cm^{-1}. XRD patterns of the mixed halide perovskite structure of MAPbIBr$_2$ sample (Red lines) is exhibited that the crystalline structure of the layers had the cubic MAPbBr$_3$ phase at the reflections positions (Red bars) of (100) and (200) [14,8] as shown in figure (4). The sample is achieved by deposited perovskite precursor solution using drop casting process on glass substrate and annealing at 100 °C. Figure(4) depicts the XRD pattern of MAPbICl$_2$ thin film (blue line), which achieved by deposited perovskite precursor solution via using drop casting process on glass substrate and annealing at 100 °C. The reflections are indicated to the tetragonal MAPbI$_3$. Reflections positions (blue bars) of (110) and (220) corresponding with tetragonal structure are indicated by ref [8 15] for comparative. XRD patterns of the mixed halide perovskite structure of MAPbICl$_2$ sample annealed at 100 °C, blue line curve, is exhibited the tetragonal MAPbI$_3$ phase and can be confirmed by reflections positions of (110) and (220) [12 16]. The structure parameters a, b , c, α, β and γ which estimated of XRD data are inserted in table 1. Figure (5) shows the patterns XRD of the thin film of Cu$_2$O on FTO electrode which was preparation by (EPD) technique Followed by dipping in deionized water and dipping in 0.4M of CuS aqueous solution and annealing to 100 °C at 15 min. The XRD patterns of the sample preparation appear with red curve line in the figure (5) the sample good quality coated with (EPD) technique. It has strongest pattern lines in the coated sample are (110), (101), (200), (211), (310) and (301) at 2θ = 26.578°, 33.772, 37.768°, 51.755, 62.004 and 65.740°, respectively which is corresponding to SnO2(JCPDS-ICDD files # 46-1088). The sample coating have another strong pattern appeared in peaks are (110), (111), (200) and (220) at angle 2θ = 29.981°, 37.768°, 42.811o and 62.004o which is identify for the Cu2O(JCPDS-ICDD file # 34-1354) on the sequences, as shown as in figure(5). Figure (6) shows the high-resolution Scanning Electron Micrographs (SEM) images of thin film of Cu$_2$O has been electrophoretically deposited (EPD) on FTO electrode, the (SEM) images of which clearly shows the transformation from particles to aggregations structure. As can be seen from these micrographs, the structure of particles are nearly spherical in shape with reasonably uniform size distributions size (0.8- 1.5)μm. scale bars of the images are (10 and 50)μm, scanning with high voltage

5kV and magnification (5 and 1) kx, respectively. The uniform deposition and the penetration of Cu_2O on FTO electrode could be seen in the Figure(6).

Optical Studies

Figure 7(a) is illustrated the absorption of halide perovskite films and it clears more absorption to $MAPbICl_2$ than the sample $MAPbIBr_2$ that which are measured in the wavelength range (400-800) nm using a (SPECTRO UV/VIS Double Beam (UVD-3500) Labomed, Inc.) and glass substrates as reference samples. Plots inset of $(\alpha h v)^2$ versus photon energy (hv) for the films peroveskite deposited on glass substrates are estimated of Absorption charts of the film with the thick (400nm) as shown in Figure 7(b). A direct optical band gap energy (E_g) for halide perovskites materials $MAPbX_3$, (X = Cl, Br, I) is reported by Simon et al [17]. Energy gap (Eg) of both samples is determined by fitting the absorption data to the direct transition equation (4). The optical band gap value is estimated by extrapolating the linear part of the curve $(\alpha h v)2$ as a function of photon energy, hv , intercept with the (hv) axis at $\alpha =$ 0. The values of Eg of MAPbICl2 and MAPbIBr2 via data UV-Vis are estimated (1.7 and 2.05)eV, respectively, as shown in figure 7b and table 1.

Figure 8(a,b) is illustrated the HOMO and LUMO distribution for density of states (DOS) as function of electrons orbitals energy of $MAPbICl_2$. Figure 8(c, d) is depicted HOMO and LUMO distribution for the (DOS) as function of electrons orbitals energy of MAPbIBr2. Transparent green and brown color orbital's are indicated to α and β electrons, (electron at spin +1/2 and electron at spin -1/2), respectively. DOSs plots of figure 9(a) are computed of molecular $MAPbICl_2$ for orbitals 4Py and 2S of Pb anion, 5Pz and 5Px of N anion and 3Py of Br cation of $MAPbIBr_2$ at unit cell. The energy gap (Eg) of $MAIPbCl_2$ between HOMO and LUMO which is estimated (2.0565)eV which is identify of the empirical value of optical energy gap of $MAPb(I_xCl_{1-x})_3$, as reported, Eg = 1.64eV [17], as shown in figure 9(a) and table 1. An additional, the evaluations the energy levels of initial tail states of HOMO and LUMO are determined at (-5.628) eV and (-3.5715) eV, respectively. We are used the ground state energy of Hartree-Fock method and SDD built-in basis set in Gaussian 09 for all orbitals type due to heavy Pb element. Figure 9(b) plot is depicted DOS as function of energy of unit cell of $MAIPbBr_2$. At the same previous method of theoretically computed calculations of Gaussian program, E_g of $MAIPbBr_2$ is (1.8113) eV. An additional, the evaluated the energy levels of initial tail states of HOMO and LUMO are determined (-5.68525) eV and (-3.87219) eV, respectively, as shown in figure 9(b) and table 1. Naveen Kumar Elumalai et al. were studied the properties of different materials of photovoltaic perovskite in the progress presently decade, they were reported that HOMO and LUMO electrons levels of $MAPbBrI_2$ were (-5.4 and, -3.6) eV, respectively [18].
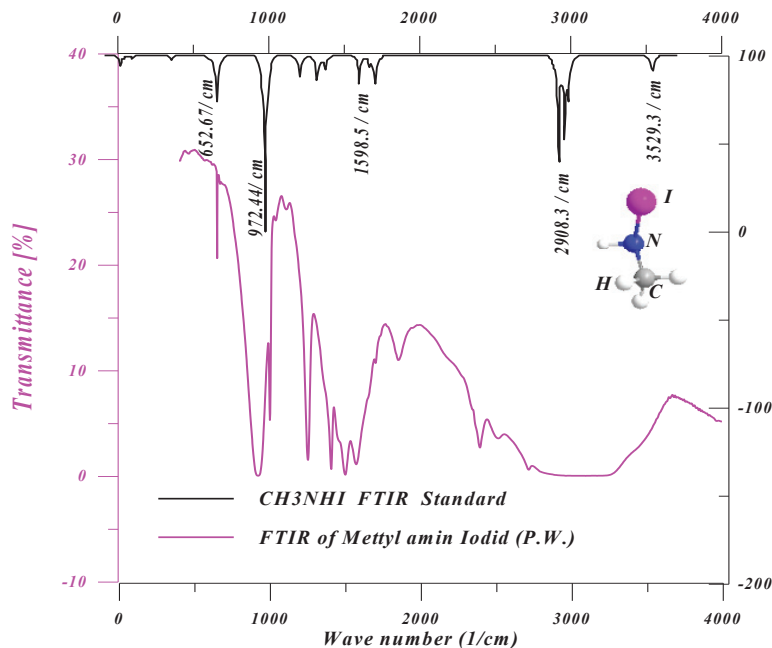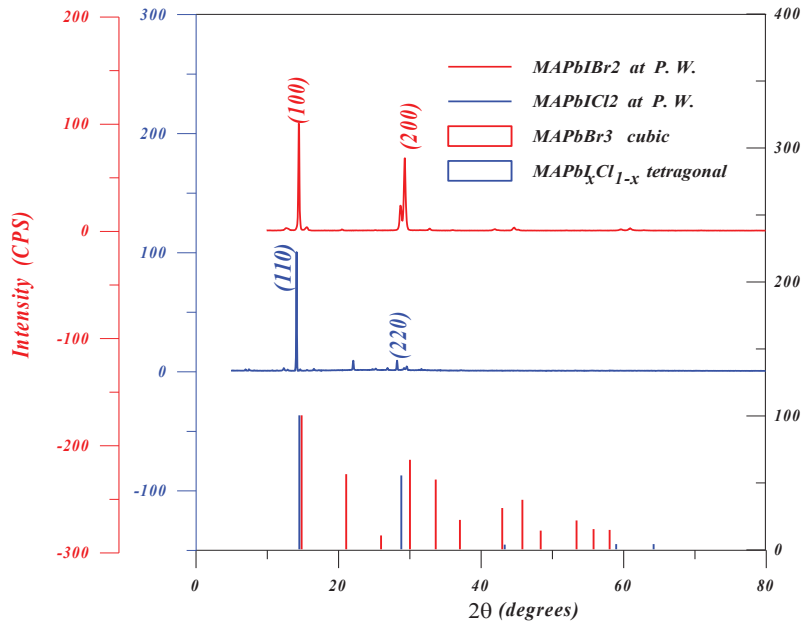

FIGURE 3. FTIR Spectral of MAI powder.

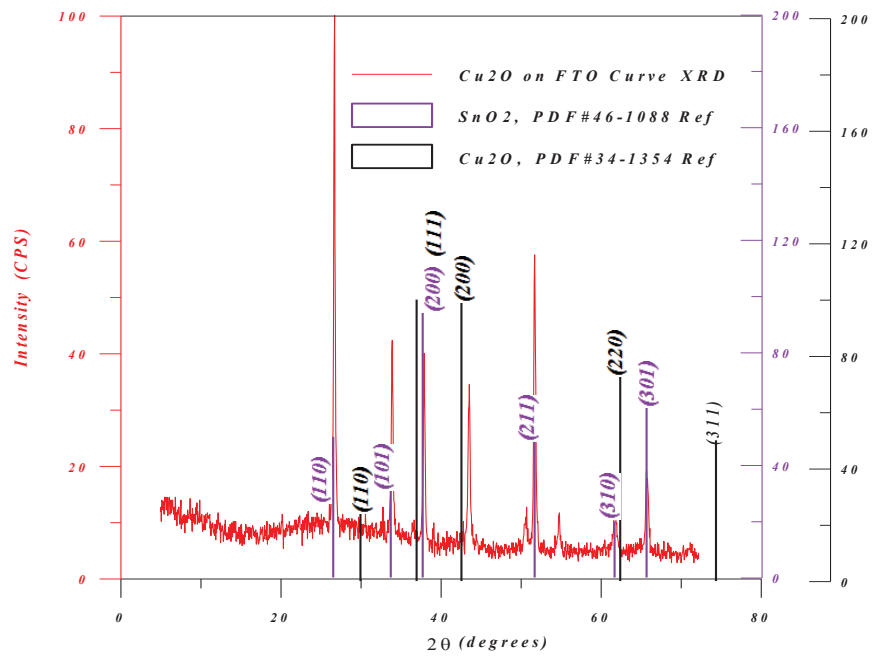**FIGURE 4.** XRD Pattern of perovskite thin films.
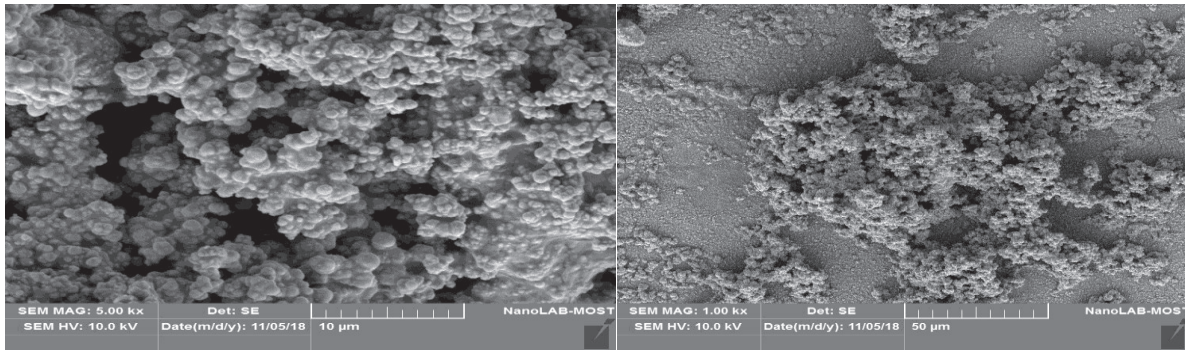

FIGURE 5. XRD Pattern of Cu2O on FTO thin films.

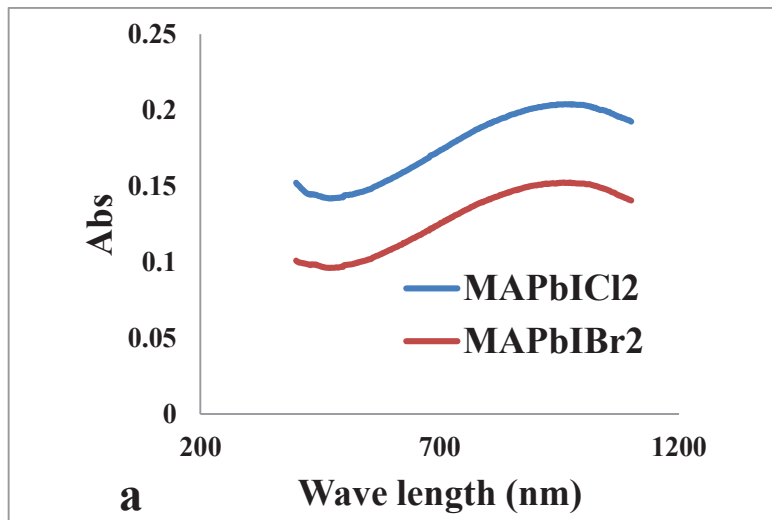**FIGURE 6.** Top SEM images thin film of Cu_2O deposited (EPD) on FTO electrode.

(a)
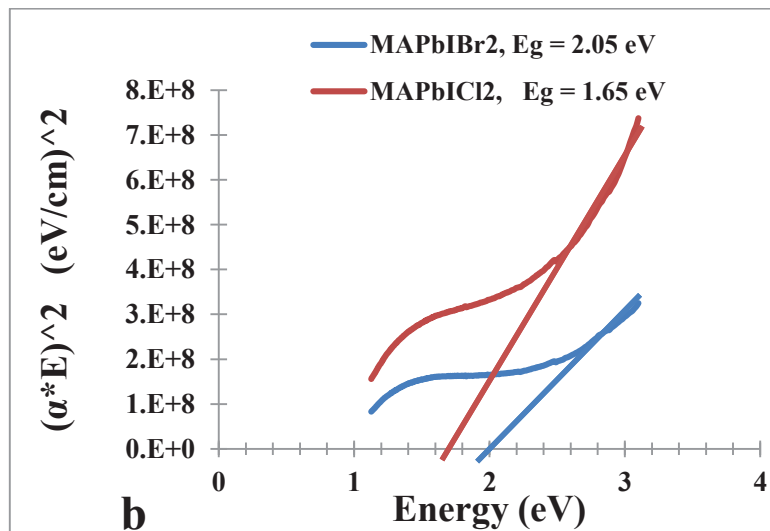
(b)

FIGURE 7. Optical properties of $MAPbIX_2$, x=Br or Cl, a). Absorption. b). Energy gap.

FIGURE 8. (a and b). DOS of HOMO and LUMO levels of MAPbICl₂, (c and d). DOS of HOMO and LUMO levels of MAPbIBr₂, Transparent green and brown color orbitals are indicated to α and β electrons.

FIGURE 9. (a). DOS of electrons levels of MAPbICl, (b). DOS of electrons levels of MAPbIBr2.

TABLE 1. Optical and structural properties of Perovskite materials style.

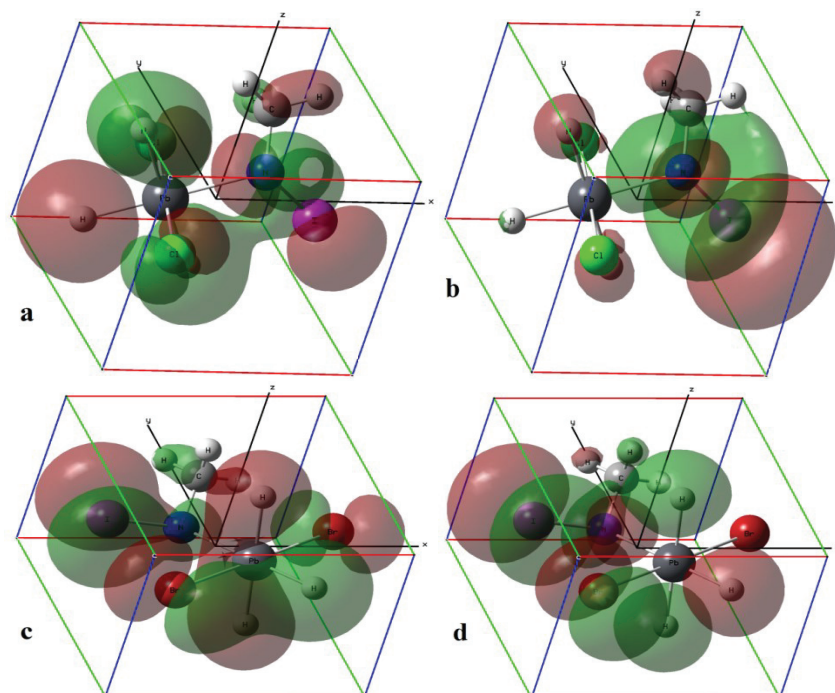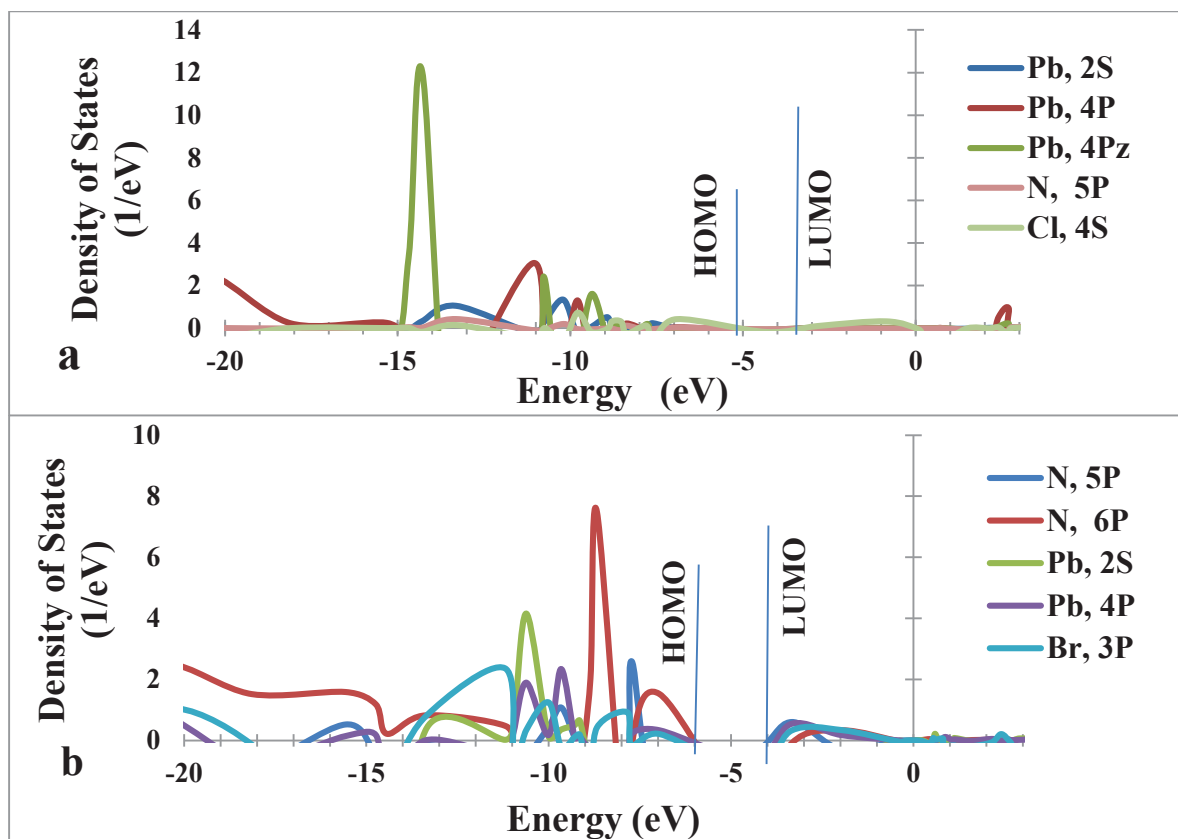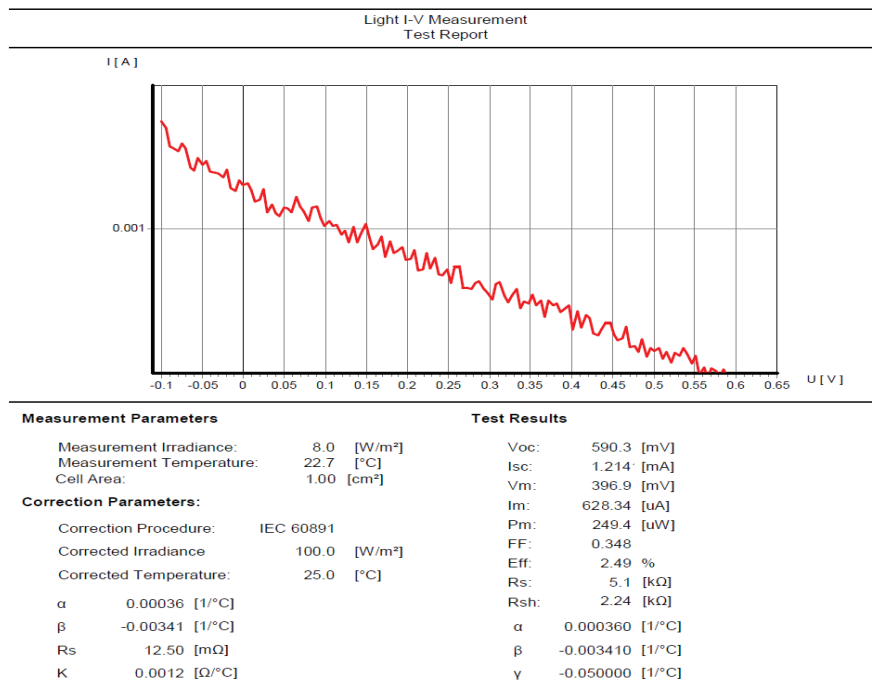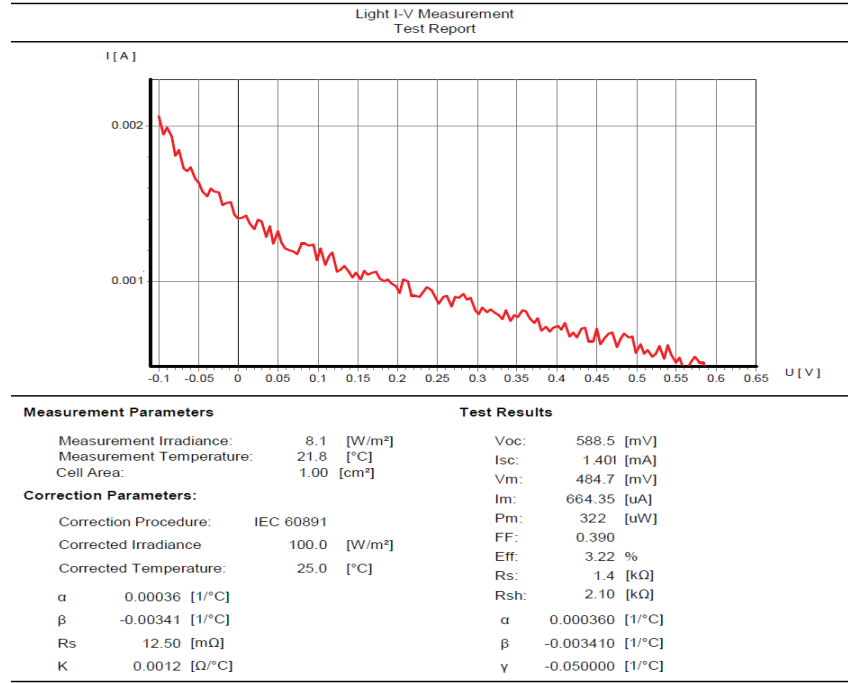| Optical Properties	MAPbIBr$_2$		MAPbICl$_2$	
	Theoretical compute	Experimental data	Theoretical compute	Experimental data
HOMO	-5.852 eV	-5.4 eV [17]	-5.628eV	MAPb(IxCLx-1)3 -5.3 eV [18]
LUMO	-3.872 eV	-3.6 eV [17]	-3.5715 eV	MAPb(IxCLx-1)3 -3.75 eV [18]
Eg	1.98 eV	2.05 eV P.W. 1.8 eV [17]	2.0565 eV	1.65 eV P.W. 1.55 eV [18]
Structural Properties	Theoretical compute	Experimental data of XRD	Theoretical compute	Experimental data of XRD
	Orthorhombic	Cubic	Orthorhombic	Tetragonal
a (A°)	6.3799987	6.07058	5.9928344	5.91
b (A°)	6.5223345	6.07058	5.8297582	5.91
c(A°)	4.6050049	6.07058	5.4201503	5.94
α	90	90	90	90
β	90	90	90	90
γ	90	90	90	90

Performance of P.V. Devices Studies

The measurements of I-V curve of (OPSC) that employed of MAPbIBr$_2$ as absorption layer of photovoltaic device have best PCE and it is depicted in figure (10.a). The measurement is carried out under intensity illumination (100 W/m^2), active area of solar cell is 1 cm^2 and sweeping voltages in the scan-direction with a scan rate of s = 50 mV/s. Figure (10.b) is depicting I-V curves of photovoltaic device that employed of MAPbICl$_2$ as absorption layer. The measurements are testing at the same conditions in the figure (10.a). All of the parameters of the performance OPSCs are inserted in the table (2). The best efficiency (PCE = 3.22) is achieved to the OPSC employing MAPbIBr2 as sensitizer due to the best optical properties, higher absorption and lower optical energy gap, than absorption layer MAPbICl$_2$, as shown in figure (7) and table (2).

Light I-V Measurement Test Report

Measurement Parameters

Measurement Irradiance: 8.0 [W/m²]
Measurement Temperature: 22.7 [°C]
Cell Area: 1.00 [cm²]

Correction Parameters:

Correction Procedure: IEC 60891
Corrected Irradiance: 100.0 [W/m²]
Corrected Temperature: 25.0 [°C]

α 0.00036 [1/°C]
β -0.00341 [1/°C]
Rs 12.50 [mΩ]
K 0.0012 [Ω/°C]

Test Results

Voc: 590.3 [mV]
Isc: 1.214 [mA]
Vm: 396.9 [mV]
Im: 628.34 [uA]
Pm: 249.4 [uW]
FF: 0.348
Eff: 2.49 %
Rs: 5.1 [kΩ]
Rsh: 2.24 [kΩ]

α 0.000360 [1/°C]
β -0.003410 [1/°C]
γ -0.050000 [1/°C]

(a)

FIGURE 10. I-V curve of OPSC have MAPbIBr2 & MAPbICl2 as absorption layer of PV device, respectively.

Light I-V Measurement
Test Report

Measurement Parameters

Measurement Irradiance:	8.1	[W/m²]
Measurement Temperature:	21.8	[°C]
Cell Area:	1.00	[cm²]

Correction Parameters:

Correction Procedure:	IEC 60891	
Corrected Irradiance	100.0	[W/m²]
Corrected Temperature:	25.0	[°C]
α	0.00036	[1/°C]
β	-0.00341	[1/°C]
Rs	12.50	[mΩ]
K	0.0012	[Ω/°C]

Test Results

Voc:	588.5	[mV]
Isc:	1.401	[mA]
Vm:	484.7	[mV]
Im:	664.35	[uA]
Pm:	322	[uW]
FF:	0.390	
Eff:	3.22	%
Rs:	1.4	[kΩ]
Rsh:	2.10	[kΩ]
α	0.000360	[1/°C]
β	-0.003410	[1/°C]
γ	-0.050000	[1/°C]

(b)

FIGURE 10 Continued. (a&b). I-V curve of OPSC have $MAPbIBr_2$ & $MAPbICl_2$ as absorption layer of PV device, respectively.

TABLE 2. Preferences parameters of OPSCs.

OPSCs	V_{oc}(mV)	I_{sh}(mA)	V_m(mV)	I_m(mA)	P_m(µW)	FF	E_{ff} %	R_s(kΩ)	R_{sh}(kΩ)
MAPbIBr	588.5	1.401	484.7	0.664	322	0.39	3.22	1.4	2.1
MAPbICl	590.3	1.214	396.9	0.628	249.4	0.35	2.49	5.1	2.24

To shed light on figure (10) and figure (7), it can be observed that is improved PCE of OPSC when increased photocurrent density due to more absorption of perovskite layer $MAPbIBr_2$ than other perovskite layer $MAPbICl_2$ of OPSCs device. Figure (10) explained the PCE of OPSCs and appeared all the parameters (R_s, R_{sh}, FF, V_{oc}, and I_{sc}) of OPSCs which inserted in the table (2). The full factor value of solar cell device are dominated via determine the parameters series and shunt resistances (R_s and R_{sh}) of the solar cells [19,20]. Figure (11) is illustrated the bind energy diagram of OPSCs which have (a). MAPbIBr2 and (b). MAPbICl2 perovskite materials as harvester light layers. HOMO and LUMO energy levels of ZnO are (-7.7 and -4.1)eV, respectively. HOMO and LUMO energy levels of Cu2O are (-5.37 and -3.2) eV, respectively, as reported by Edson Meyer et al [21]. The conduction band of FTO electrodes is reported at (-4.4)eV [22,23]. We were employed Gaussian 09 to calculate HOMO and LUMO energy levels for perovskite materials of $MAPbIBr_2$ or $MAPbICl_2$. The Fermi level (EF) is hold fixed between energy levels of orbitals HOMO and LUMO, $E_F = (E_{HOMO}+E_{LUMO})/2$. EF of perovskite materials $CH_3NH_3PbICl_2$ was estimated (EF= -4.599 eV), and the energy levels of FTO electrodes are (-4.4 eV). The difference potential between two FTO electrodes, ($V_{oc\ th}$), of OPSC can be estimated (2.05 V) of the equation (4) when neglecting loss energy ($V_{oc\ th} = E_g/e$). The empirical value of ($V_{oc\ exp}$) of OPSC with $CH_3NH_3PbICl_2$ as harvesting light layer is (0.5903 V), as the shown in the table(2), then E_{loss} can be estimated (1.06 eV) of $E_{loss} = qV_{oc(th)} - q\ V_{oc(exp)}$, table (3). As the same method, we estimated the E_F, E_{loss}, and $V_{oc(th)}$ of the performance of OPSC had $CH_3NH_3PbIBr_2$ as harvester light layer and inserted in the table(3). From the table (3), it can be observed that Eloss is very high value and more evaluated $V_{oc(th)}$ than $V_{oc(exp)}$ due to that may be the several junctions of the configuration device of OPSCs (6 junctions), as shown in the figure (11). Eloss of OPSC had $MAPbIBr_2$ as harvester light layer is (1.462) eV, as shown in the table (3), then (E_{loss} = 0.243 eV) per junction. This result is a like with to which report by Tsutomu Miyasaka that the charge transfer across solid-solid hetero junctions which normally undergoes an energy loss of (E_{loss} > 0.2) eV per junction [24,25]. An addition, the possible of the loss energy via to be the incomplete contact of FTO electrodes with the external electric circuit.
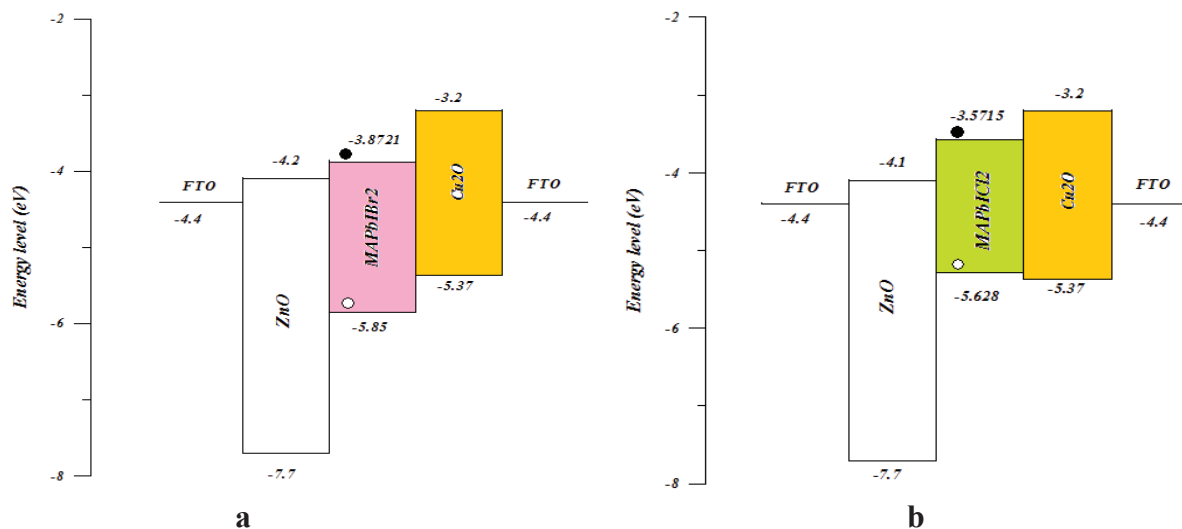
FIGURE 11. Bind energy diagram of OPSCs have, (a). $MAPbIBr_2$ or (b). $MAPbICl_2$, as harvester light layer.

TABLE 3 Comparative studying of theoretical and imperial performance of OPSCs.

OPSCs	E_F(eV)	E_g(eV)	Voc th (V)	Voc exp (V)	E_{Loss}(eV)
$MAPbICl_2$	-4.599	1.65	1.65	0.5903	1.06
$MAPbIBr_2$	-4.8721	2.05	2.05	0.5885	1.462

CONCLUSION

In this paper, the OPSCs with construction (FTO/ZnO/$MAPbIX_2$ perovskite with Al_2O_3 scaffold/Cu_2O/FTO electrode), X= Br or Cl, have been successfully fabricated. The empirical results give an optimum PCE = 3.22 % can be achieved by using $MAPbIBr_2$ as harvesting light layer in OPSC. In addition, we show to employ the simulation of the software Gaussian 09 program in improved of the description empirical results. Although of the density function theory act in a Hartree-fock method gives 9% of rate error, we can be neglecting in the estimated HOMO, LUMO energy levels and HOMO-LUMO energy gap due to give approximately description of the experimental results. We can observed that the PCE of the OPSC have $MAPbIBr_2$ is more than the PCE of OPSC with $MAPbICl_2$ as absorption layer, as shown in table (3), because of resulted from the better matched valence band of Cu_2O a with that of the valance bond of $MAPbIBr_2$ than other perovskite ($MAPbICl_2$), as shown in the figure (11). As observed remarks, the rates error between the empirical results and theoretical results, Gaussian 09 program results, of lattice parameters (a, b and c) of the crystalline structure of $MAPbIBr_2$ are acceptable rates, (1%, 1% and 8%), respectively, then lower than the rates error in the structure of $MAPbICl_2$ are (5%, 7% and 24%), respectively. In the current work, the achieved experimental data of OPSCs have been enhanced with Computational studies of Gaussian 09 program result.

ACKNOWLEDGEMENTS

REFERENCES

1. J. Fan, B. Jia, M. Gu, Photonics Res. **2**, 111-120 (2014).
2. Diau , Chen, "Perovskite Solar Cells, Principle, Materials and Device". (World Scientific Publishing Co. Pte. Ltd; 2017).
3. Y. Ye, X. Run, X. Hai-tao, H. Feng, Chin. Phys. B, **24**, 116302 (2015).
4. J. Even, L.Pedesseau, C.Katan, et al, Photonics for Solar Energy Systems V **9140**, 91400Y (2014).

5. A. M. Jafar, K. Al-amara ,L.F. Rashid, I.K. Fayyadh, Journal of Innovative Research in Engineering & Science **6**, 49-58 (2013).
6. A.M.Jafar, K.Al-amara, T.M. Lafta, M.H. Mahmod, I.M. Abood. Thin Film Technology **65**, 9799-19803 (2013).
7. A. Ravikumar, A. Baby, H. Lin, G. P.Brivio, G.Fratesi, Sci Rep. **6**, 24603 (2016).
8. A. M. Jafar. "Fabrication and Characterization of Perovskite Solar Cells" (Minist High Educ Sci Res Univ Baghdad Coll Sci. 2017).
9. A. M. Jafar, M.H.Suhail, F.M.Al-Attar. (32nd European Photovoltaic Solar Energy Conference and Exhibition 32st. Munich - Germany).
10. A. M. Jafar, M.H.Suhyl, F.I.Mustafa. J. Energy **2**, 81-87 (2015).
11. M. H. Suhail and A.M.Jafar. Renewable Energy **98**, 42709-42713 (2016).
12. R. D. Corpuz, J.R.Albia, Mater Res. **17**, 851-856 (2014).
13. H. Zhen-hua, Z.Jian-jun, N.Jian, Chin. Phys. B **27**, 024208 (2018)
14. D. Priante, I. Dursun, M.S. Alias, S. Shi, V.A. Melnikov, T.K. Ng, O.F. Mohammed, O.M. Bakr, and B.S. Ooi, Applied Physics Letters, **106**, 081902 (2015).
15. T. Oku, "Crystal structures of CH3NH3PbI3 and related perovskite compounds used for solar cells" (Solar Cells-New Approaches and Reviews, 2015).
16. S. Chavhan, O. Miguel, H.J. Grande, V. Gonzalez-Pedro, R.S. Sánchez, E.M. Barea, I. Mora-Seró, and R. Tena-Zaera, Mater Chem A. **2**, 12754-12760 (2014).
17. N. K. Elumalai, A.Mahmud, D.Wang, A.Uddin, Energies **9**, 861 (2016).
18. S.A.Bretschneider, J.Weickert, J.A.Dorman, L.Schmidt-Mende, APL Mater **2**, 040701 (2014).
19. G.Sissoko, S.Mbodji, Int J Pure Appl Sci Technol. 103-114 6, (2011).
20. L. Etgar, Materials **6**, 445-459 (2013).
21. E. Meyer, D.Mutukwa, N.Zingwe, R.Taziwa, Metals **8**, 667 (2018).
22. H. S. Jung, N.G.Park, small **11**, 10-25. (2015).
23. M. K. Assadi, S. Bakhoda, R. Saidur, H.Hanaei, Renew Sustain Energy Rev. 295, 2812-2822 (2018),
24. A. Ishii, A.K.Jena, T.Miyasaka APL Mater. **2**, 091102 (2016).
25. T. Miyasaka, "Hybrid Photovoltaic Cells Based on Organo Metal Halide Perovskite with Crystalline and Noncrystalline Conductors," (International Conference on Hybrid and Organic Photovoltaics, 2019).